

\mathcal{H}_∞ Reduced Order Control for Nanopositioning: Numerical Implementability

Michael R. P. Ragazzon* Arnfinn A. Eielsen*
J. Tommy Gravdahl*

* *Department of Engineering Cybernetics, Norwegian University of
Science and Technology, Trondheim, Norway*
(e-mail: {ragazzon, eielsen, Tommy.Gravdahl}@itk.ntnu.no)

Abstract:

In this paper we discuss how model reduction affects the stability and computational complexity of controllers for nanopositioning systems. A robust \mathcal{H}_∞ multiple-input multiple-output controller is designed and implemented for the lateral stage of an atomic force microscope. A model-based controller can often be of high order and may be difficult to run in real-time on hardware with limited computational power. The resulting controller can be considered to be stiff, which is characterized by a large spread of eigenvalues. Continuous-time systems running in real-time are often solved using explicit Runge-Kutta (ERK) methods, which easily becomes unstable for stiff systems. We show how small the time-step for a given controller needs to be for a selection of ERK methods. We also consider how model reduction affects the computational complexity of the controller, and show how the reduction can alter the placement of the eigenvalues and thus the required step-size for implementability. We demonstrate that the original 18th-order \mathcal{H}_∞ controller can be reduced to a 10th-order controller without any significant reduction in performance or stability, which results in a 46.7% reduction in execution time, partly because the order reduction enables the use of a simpler solver type.

Keywords: Model reduction; H-infinity control; Stability of numerical methods; Runge-Kutta method; MIMO; Positioning systems.

1. INTRODUCTION

Atomic force microscopy (AFM) is a tool capable of studying and manipulating matter down to the atomic scale. This has made it one of the fundamental tools within the field of nanotechnology. Control of the lateral stage of an AFM has been shown to be challenging due to several reasons, including non-linearities such as hysteresis and creep, lightly-damped vibration dynamics, and large uncertainties. Some of these effects can be effectively compensated for such as hysteresis (Eielsen et al., 2012; Kaizuka and Siu, 1988; Croft et al., 2001). To handle the resonant peaks of the lightly-damped vibration dynamics, simpler control schemes such as damping and tracking control can be employed (Eielsen et al., 2013; Aphale et al., 2008; Fleming, 2010; Fleming et al., 2010). However, higher order model-matching based techniques, such as model reference control (MRC), linear quadratic control (LQR) and \mathcal{H}_∞ -control, can in principle allow for higher bandwidth, and can therefore lead to better tracking performance. Model-matching control, especially \mathcal{H}_∞ -control, has been widely employed in the nanopositioning literature (Schitter et al., 2001; Salapaka et al., 2002; Salapaka and Sebastian, 2003; Schitter and Stemmer, 2004; Ladjal et al., 2009; Yong et al., 2010). These controllers tend to have a high order, which in turn leads to high computational complexity. Because of the large uncertainties and the non-

linearities it is also important to consider robustness in nanopositioning applications. This topic has been studied in Salapaka et al. (2002); Sebastian and Salapaka (2005); Ladjal et al. (2009).

The majority of the literature on nanopositioning appears to perform control design in the continuous time s -domain as opposed to the discrete-time z -domain. Such controllers can be described using continuous-time state-space models which we will base our discussion on. For a real-time implementation however, the model is solved at discrete time-steps using a fixed step-size. Many popular solver types are based on the family of explicit Runge-Kutta (ERK) methods. These solvers become unstable if the step-size is too large, and the maximum step-size depends on the order of the solver used. At the same time, the complexity of the controller running on hardware with limited computational power puts a lower limit on the step-size, because the hardware needs sufficient time to perform the necessary calculations. Thus we have both a lower and an upper limit on the step-size determined by various factors. For a controller to be implementable we need the limits to intersect. In this paper we will discuss these factors and present some approaches to handle them.

To control a system with a high mechanical bandwidth, we need to have high bandwidth for the control loop as well. Thus, the step-size needs to be sufficiently small.

On hardware with limited computational power, we often need to simplify the model such that it becomes feasible. The most widely used method to reduce the computational complexity of a controller is to perform model reduction on an already existing controller. Model reduction aims to keep the input-output behavior as close as possible to the original model while removing states from a state-space representation of the controller. Model reduction has been used extensively—some approaches perform reduction on the plant model (Dong et al., 2007; Lee and Salapaka, 2009). Using a model-based approach, this results in a controller with less complexity. Another approach is to perform reduction after synthesis using a high-order model plant (Schitter and Stemmer, 2004; Kuiper and Schitter, 2012). The topic of controller reduction is treated in Anderson and Liu (1989); Anderson (1993) where it is generally concluded that reduction should be performed as a last step in the control design process. Even if the system is already implementable, there is an advantage of reducing the complexity, because we can then run the system on a smaller step-size which reduces the overall noise floor of the system (Lyons, 2010).

In this paper, we will base our discussion around a \mathcal{H}_∞ controller which is designed for the lateral positioning of a commercial AFM. The controller is designed to be robustly stable for a given description of plant uncertainty. We will present equations for how to determine the solver stability of a controller and the required maximum step-size for a variety of ERK methods. Additionally, we will show the effect of model reduction on the complex controller and how this affects the solver stability and computational complexity. This paper is based to some extent on Ragazzon (2013).

The paper is organized as follows. In Section 2, the experimental set-up is explained and an identified model of the plant is found. In Section 3, we present the controller design. In Section 4 we present solver stability, specifically for some ERK methods. Section 5 describes the model reduction of the controller. Section 6 gives experimental results of closed-loop characteristics and execution time. The results are discussed in Section 7. Finally, some conclusions are drawn in Section 8.

2. SYSTEM IDENTIFICATION

2.1 Device Description

All experiments are done using a commercial AFM of the type Park Systems XE-70. In this device, the sample is placed on a parallel kinematic flexure scanner for motion in the horizontal xy -plane. Motion along the vertical z -axis is completely decoupled and not studied in this paper. The signals from the AFM are routed to an electronic processing and controller box. As well as having its own controller circuits, it provides access to measurements from the sensors. It can also receive external control signals for manual control of the piezoelectric elements of the AFM.

A schematic overview of the setup is shown in Fig. 1. The controllers are implemented in Simulink, and using the Simulink Coder, the controllers can be run on a dedicated computer running the xPC real-time operating system. The xPC is fitted with analog-to-digital and digital-to-

analog converters. The signals from these are run through anti-aliasing and reconstruction filters implemented as 2nd order Butterworth low-pass filters with a bandwidth of 10 kHz—less than half the sample frequency.

For our purpose, we have overridden control of the piezo-actuators in the x - and y -axes. These are connected to a “PiezoDrive PDL200”, a linear voltage amplifier whose inputs are considered the inputs of the system plant $G(s)$. The voltage output from the displacement sensors in the x - and y -axes located on the AFM is used as the output of the system.

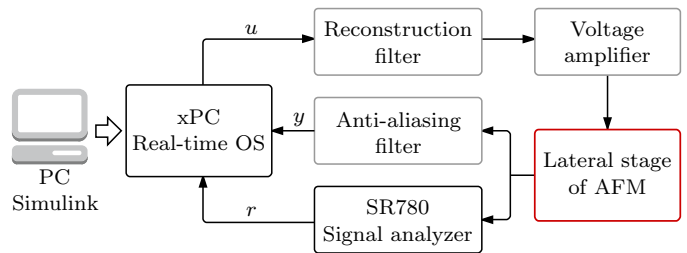


Fig. 1. Block diagram of the experimental setup for the closed-loop system. For the plant frequency response the SR780 device is connected directly to u .

2.2 Frequency Response and Model Fit

The lateral positioning stage of the AFM is considered to be dominantly linear, therefore the system can be described by its frequency response. The system has two inputs u_1, u_2 , and two outputs y_1, y_2 , along the x - and y -axis respectively. The frequency response of the plant $G(s)$ was gathered using a Stanford SR780 frequency analyzer using a white noise source signal. One of several gathered frequency responses is plotted in Fig. 2 together with the fitted models. The transfer functions were fitted using the Matlab function `tfest` on the experimental data. The diagonal elements of $G(s)$ were approximated by a third-degree transfer function, while the off-diagonal elements were approximated by a second-degree function. The identified nominal plant model is given by (1).

The exponential term represents the time-delay between input and output. A time-delay will present itself as a linear reduction of the phase as a function of frequency. Thus, we may find the time-delay of the system between input and output by investigating the phase plot of the elements of \hat{G} . By assuming that the change in phase at lower frequencies is dominated by the time-delay, and other sources of phase change is close to zero, we can deduce that the time-delay is proportional to the slope at the start of the phase plot. This is how we identified the time-delay $T_d = 4.58 \times 10^{-4}$ s.

We can see that the phase starts at 180° which means that the system has an inverse response, i.e. positive inputs give negative outputs and vice versa. This is just the sign convention of our raw data, and we decided not to change it for simplicity.

We can observe that the off-diagonal elements of $G(s)$ are relatively small compared to the diagonal elements. This indicates that the two axes are physically well decoupled, and the system is thus well suited for independent control

$$G(s) = e^{-4.58e-04s} \begin{bmatrix} \frac{-5924s^2 - 1.709e07s - 9.878e10}{s^3 + 4703s^2 + 1.82e07s + 7.806e10} & \frac{-0.04567s^2 + 69.72s - 6.043e04}{s^2 + 104.5s + 2.29e07} \\ \frac{-0.04705s^2 + 89.17s - 1.253e05}{s^2 + 134.1s + 2.288e07} & \frac{-8708s^2 + 2.618e07s - 9.214e11}{s^3 + 3.865e04s^2 + 4.379e07s + 9.44e11} \end{bmatrix} \quad (1)$$

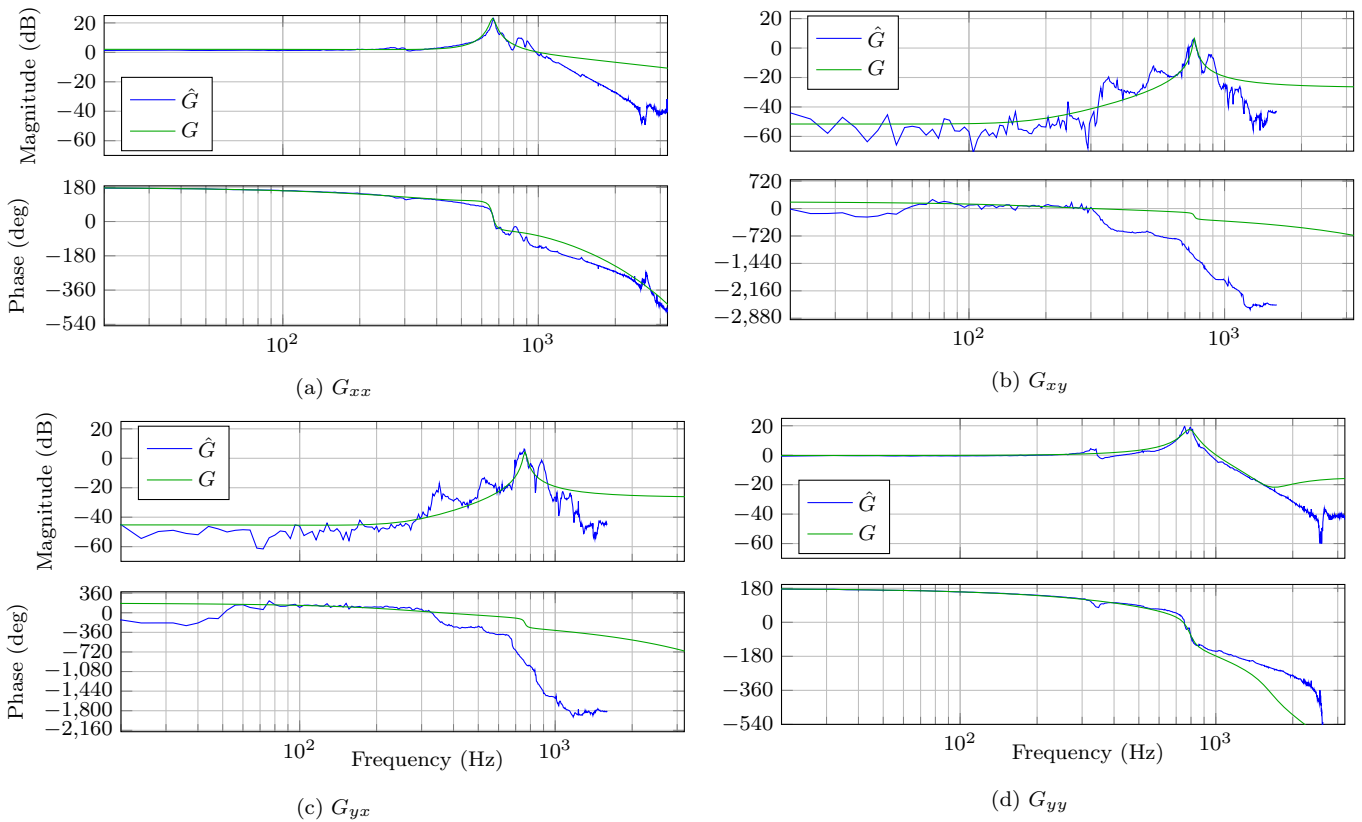


Fig. 2. Experimental frequency response for both axes including cross-terms $\hat{G}(\omega)$, and corresponding model fit $G(s)$.

of the axes where the cross-coupling is not considered. However, we will treat the system as a single multiple-input multiple-output (MIMO) plant and design a single controller rather than two independent controllers of lower order such that our design strategy and analysis is applicable in more general cases.

2.3 Robust Stability and Uncertainty Weighting

Since the system has large uncertainties and inaccuracies in the estimated model, we need to make sure it is robustly stable for a specified set of perturbations of the plant. We chose to model the uncertainties as multiplicative output uncertainty. The perturbed plant is described as

$$G_p = (I + \Delta W) G \quad (2)$$

where Δ is the uncertainty variable with $\|\Delta\|_\infty \leq 1$ and W is a specified weighting transfer function. The block-diagram of the feedback system is shown in Fig. 3.

For a given controller K the robust stability (RS) condition for the described set of perturbations is (Skogestad and Postlethwaite, 2007)

$$RS \Leftrightarrow \|WT\|_\infty < 1 \quad (3)$$

where $T \triangleq (I + GK)^{-1}GK$ is the complementary sensitivity function. Similarly we have the sensitivity function $S \triangleq (I + GK)^{-1}$.

To find a suitable W that fits the uncertainties in our system, we can record a set of plant frequency responses $\hat{G} \in \Pi$. Robust stability can be guaranteed for at least all of these responses by finding a W such that $|W(j\omega)| > \hat{W}(\omega)$ where (Skogestad and Postlethwaite, 2007)

$$\hat{W}(\omega) \triangleq \max_{\hat{G} \in \Pi} \bar{\sigma} \left(\left(\hat{G}(\omega) - G(j\omega) \right) G^{-1}(j\omega) \right) \quad (4)$$

and $\bar{\sigma}(\cdot)$ is the maximum singular value. Other equations exist for different perturbation descriptions such as input multiplicative uncertainty or additive uncertainty.

We recorded three sets of frequency responses at different set-points and input amplitudes, and fitted the calculated \hat{W} by the transfer function

$$W(s) = 3.8254 \frac{(s + 210)(s + 1850)}{(s + 2400)(s + 3200)} \quad (5)$$

which is plotted together with \hat{W} in Fig. 4.

3. CONTROLLER DESIGN

This Section will present the design of the \mathcal{H}_∞ controller. We will explain the choice of weightings for the mixed-sensitivity problem used to synthesize the controller based on the identified model G .

The \mathcal{H}_∞ mixed sensitivity problem can be formulated as

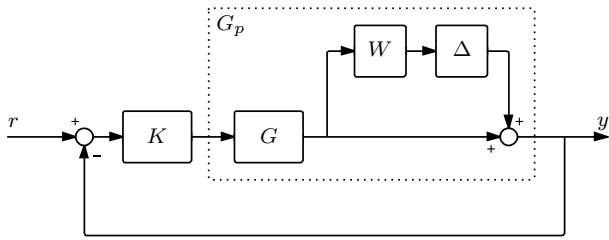


Fig. 3. Feedback system with a multiplicative output uncertainty

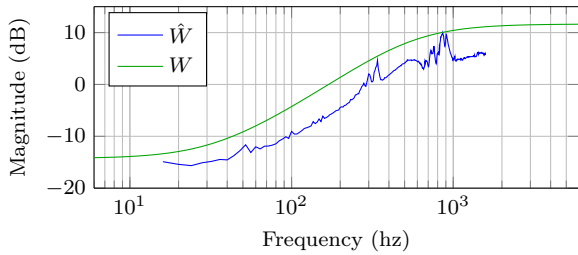


Fig. 4. Robustness fit, $W(s)$ and $\hat{W}(\omega)$

$$\min_K N(K) = \left\| \begin{array}{c} W_1 S \\ W_2 T \\ W_3 K S \end{array} \right\|_{\infty} \quad (6)$$

where the transfer functions W_1 , W_2 , and W_3 are user-defined weightings.

The sensitivity function S is the closed-loop transfer function from r to $e \triangleq y - r$. We want this to be as small as possible within the desired bandwidth for effective control. Thus, W_1 was chosen as a first-order filter with large gains at low frequencies and low gains at high frequencies.

The complementary sensitivity function T is the closed-loop transfer function from r to y . We would like this to be close to unity within the desired bandwidth for good tracking behavior. For higher frequencies we would like it to be as small as possible to attenuate measurement noise. Thus W_2 is chosen to be small at low frequencies and large at high frequencies. Since WT is a measurement of the robust stability we have chosen $W_2 = W$ to shape the system such that it becomes more easily robustly stable.

Finally, we have the weighting W_3 . In fact, KS is the closed-loop transfer function from r to u , so it describes the control effort for a given reference signal. We want to reduce high frequencies in the control signal u in order to reduce the energy usage by the controller. Thus W_3 is chosen as a high-pass filter. The resulting weighting functions are summarized in Table 1.

The synthesis problem was solved using the Matlab function `mixsyn`. This resulted in a controller with 18 states. For the sake of comparison later on, we also designed a similar controller using independent axis design, i.e. one \mathcal{H}_{∞} controller for each axis (denoted \mathcal{H}_{∞} SISO), as well as a simple PID controller. The bandwidth of all three controllers as well as the robustness properties and model order is given in Table 2. The table shows that the closed-loop system is robustly stable because $\|WT\|_{\infty} < 1$ for both of the \mathcal{H}_{∞} controllers. This is not the case for the PID-controller, thus we can not guarantee this controller to be stable for all perturbations of the system.

The bandwidth of the \mathcal{H}_{∞} controllers were severely limited by the time-delay of the system. Higher bandwidth resulted in bad performance in the closed-loop system which was seen as large spikes in $\bar{\sigma}(S)$ and $\bar{\sigma}(T)$.

Table 1. Summary of weighting transfer functions

$W_1(s)$	$\frac{0.8333s + 439.8}{s + 0.04398}$
$W_2(s)$	$3.8254 \frac{(s + 210)(s + 1850)}{(s + 2400)(s + 3200)}$
$W_3(s)$	$0.8333 \frac{s}{s + 439.8}$

Table 2. Bandwidth and robustness comparison of the three controllers, where ω_{BS} is the bandwidth in terms of S and ω_{BT} is the bandwidth in terms of T .

	ω_{BS} [Hz]	ω_{BT} [Hz]	$\ WT\ _{\infty}$	Model order
PID	58.0	93.1	1.073	4th-order
\mathcal{H}_{∞} SISO	75.6	96.4	0.9938	14th-order
\mathcal{H}_{∞} MIMO	69.8	98.6	0.6717	18th-order

4. SOLVER STABILITY

We will consider the case where a controller is represented by a continuous-time state-space model. A real-time implementation of such a model will use a solver to perform the necessary integration steps at fixed discrete time intervals, denoted by the step-size h . In this section we will see that the solver stability depends on the eigenvalues of the controller, the step-size, as well as the solver type.

Let us consider the scalar test system

$$\dot{y} = \lambda y \quad (7)$$

which is applied to a solver taking the discrete state y_n to the next time step y_{n+1} with step-size h ,

$$y_{n+1} = \Phi(h\lambda)y_n \quad (8)$$

$$= [\Phi(h\lambda)]^n y_0 \quad (9)$$

where $\Phi(h\lambda)$ is called the stability function. It is evident that (9) is stable, i.e. $|y_n| \leq c < \infty \forall n \geq 0$, if and only if

$$|\Phi(h\lambda)| \leq 1 \quad (10)$$

All solvers we will consider have such a stability function, and the region of stability, i.e. the region of the complex plane where (10) is satisfied, varies between each solver type.

4.1 Runge-Kutta Methods

The family of explicit Runge-Kutta (ERK) methods can be written as

$$y_{n+1} = y_n + \sum_{i=1}^s b_i k_i \quad (11)$$

where s describes the number of stages of the Runge-Kutta method and

$$k_1 = hf(t_n, y_n)$$

$$k_2 = hf(t_n + c_2 h, y_n + a_{21} k_1)$$

$$k_3 = hf(t_n + c_3 h, y_n + a_{31} k_1 + a_{32} k_2)$$

$$\vdots$$

$$k_s = hf(t_n + c_s h, y_n + a_{s1} k_1 + a_{s2} k_2 + \dots + a_{s,s-1} k_{s-1})$$

where the coefficients a_{ij} , b_i , and c_i are elements of A , b , and c respectively, which are specified by a given ERK solver.

4.2 Stability of Explicit Runge-Kutta Methods

The stability function of ERK methods are given by (Egeland and Gravdahl, 2002)

$$\Phi(z) = \det(I - zA + z\mathbf{1}b^T) \quad (12)$$

where $\mathbf{1}$ is a column vector of unit elements. An ERK method is said to be of order p if the error between the computed solution and the exact solution starting at initial time is bounded by $\mathcal{O}(h^p)$. The stability function of an ERK method of order $p = s$ can be simplified to (Hairer and Wanner, 1996)

$$\Phi(z) = 1 + z + \dots + \frac{z^p}{p!} \quad (13)$$

which is only possible for methods of order up to 4. Higher order ERK methods need more stages s than the order p . We have plotted the stability region of a selection of ERK methods in Fig. 5. Specifically the region of erk1-erk4 with $p = s$, Dormand-Prince 5 (erk5) and Dormand-Prince 8 (erk8). The last two with coefficients taken from Dormand and Prince (1980); Prince and Dormand (1981). The stability functions of these methods are reckoned to be the same as for the fixed-step solver methods available in Simulink.

4.3 Linear System

The stability properties of ERK methods applied to a scalar test system has been determined. Now we will consider the linear system of ordinary differential equations

$$\dot{y} = Ay \quad (14)$$

where A is an $n \times n$ diagonalizable matrix with eigenvalues $\lambda_1, \dots, \lambda_n$. It can be shown that the origin of this system is numerically stable if and only if all the eigenvalues λ_i satisfy (10) individually for a given solver method. This is a standard result in the literature on numerical methods, see e.g. Ascher and Petzold (1998).

In other words, if all the eigenvalues of A are within the region of stability for a given solver at a specific step-size h , then the solver applied to (14) is stable. This gives us a tool to find the required maximum step-size for a given controller and solver.

5. CONTROL ORDER REDUCTION

5.1 Model Reduction Theory

There exist several methods to perform model reduction (Obinata and Anderson, 2001). The most widely used method is possibly balanced residualization. Here the controller is first transformed to a balanced realization where the model states are ordered by decreasing Hankel singular values to form a state-space model (A, B, C, D) . The last states are removed and the system is transformed such that

$$\left[\begin{array}{cc|c} A_{11} & A_{12} & B_1 \\ A_{21} & A_{22} & B_2 \\ \hline C_1 & C_2 & D \end{array} \right] \Rightarrow \left[\begin{array}{cc|c} A_{11} - A_{12}A_{22}^{-1}A_{21} & B_1 - A_{21}A_{22}^{-1}B_2 \\ \hline C_1 - C_2A_{22}^{-1}A_{21} & D - C_2A_{22}^{-1}B_2 \end{array} \right]$$

The DC-gain of the system is maintained using this method, at some cost to the accuracy in the faster modes. Other methods include the truncation method which is

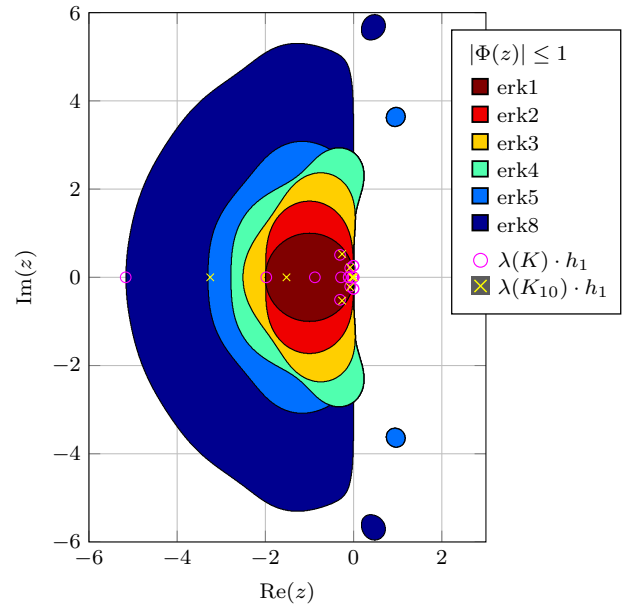


Fig. 5. Stability region of several ERK methods of order 1-5 and 8. *Magenta circles*: Eigenvalues of the full order controller K scaled by the maximum step-size achieving stability for erk8. *Yellow X's*: Eigenvalues of the reduced 10th-order controller K_{10} scaled by the same step-size. Note that K_{10} is stable for erk5.

more accurate at high frequencies at the cost of poor accuracy at low frequencies, as well as the optimal Hankel norm method and methods using linear matrix inequalities.

5.2 Results of Controller Reduction

The designed controller K was first transformed to a balanced realization using the Matlab command `balreal`. We then performed model reduction on K by model residualization to several new controllers K_r of order 2 to order 17. This was done in Matlab with the command `modred`. The closed-loop \mathcal{H}_∞ error norm on $T - T_r$, where T_r is the complementary sensitivity of the reduced controller, for each reduced controller is shown in Fig. 6a. We can see that there are significant drops specifically between order 4-5, 9-10, and 16-17. The error changes relatively little in-between these drops. Since we would like a controller with as low order as possible while maintaining the performance characteristics, we are inclined to select one of the orders after such a drop, i.e. 5, 10, or 17. The robustness norm is shown in Fig. 6b where we can see that only controller order 10 and higher are robustly stable with $\|WT_r\|_\infty < 1$. The previous discussion clearly favors choosing the 10th-order controller as it provides robust stability with little error. This choice is further reinforced by considering the simulated step responses as shown in Fig. 7. The 10th-order controller gives nearly indistinguishable results to the original controller, while the 8th-order controller show some oscillatory behavior. The 7th-order model is not internally stable, so we clearly want to avoid it.

5.3 Eigenvalues and Maximum Step-Size

We have previously seen that the stability of an explicit Runge-Kutta method applied to a state-space model de-

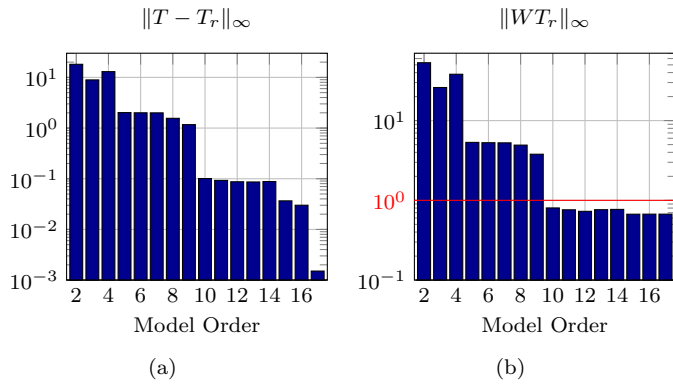


Fig. 6. Reduced controller order properties. **(a)** Closed-loop error $\|T - T_r\|_\infty$. **(b)** Robustness $\|WT_r\|_\infty$, must be < 1 for robust stability (marked red).

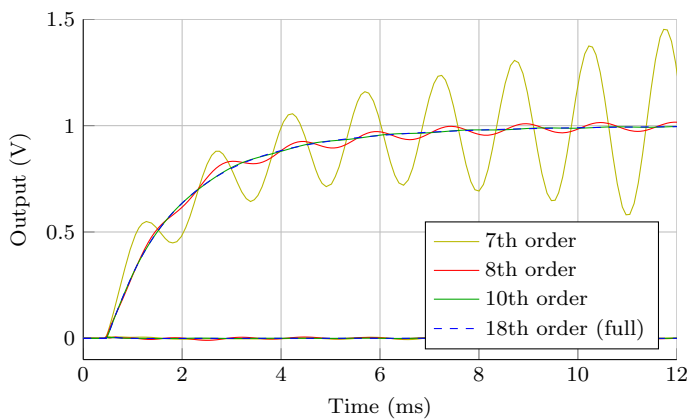


Fig. 7. Simulated step-response in reference signal on the x -axis for various reduced controllers. Shows output from both x - and y -axes.

depends on the eigenvalues of the A -matrix and the step-size. Thus, for a given controller we can find the maximum step-size needed for stability. The maximum step-size for controller K was found to be $54.62 \mu\text{s}$ using the erk8 solver. The eigenvalues scaled by step-size can be seen in Fig. 5 (magenta circles) which are seen to lie within the stability region of erk8. It is not stable for erk5 as the eigenvalues are outside the stability region for this solver. The eigenvalues of the reduced controller K_{10} has also been plotted (yellow x's) for the same step-size and we can see how the controller reduction has affected the eigenvalues. We can see that they have become smaller which has resulted in the controller becoming stable even for the erk5 solver. So not only does model reduction reduce the computational complexity of the controller, but it can also enable us to use a simpler solver type or alternatively a larger step-size.

The maximum step-size for a variety of controllers and solver types are shown in Table 3. Note that the maximum step-size does not strictly increase with lower model-orders, since the model residualization method used does not necessarily reduce the eigenvalues.

6. EXPERIMENTAL RESULTS

Experiments were performed for two reasons. The first was to see how well the reduced order controllers performed

Table 3. Maximum step-size for a given explicit Runge-Kutta (ERK) method for the various reduced controllers as well as some simpler controllers. Larger values are generally better because they are stable at higher step-sizes.

Order	$h_{max} [\mu\text{s}]$					
	erk1	erk2	erk3	erk4	erk5	erk8
7 (unst.)	32.18	71.33	95.74	100.8	127.2	203.6
8	58.37	58.37	73.34	81.29	96.51	150.8
9	37.54	37.54	47.17	52.28	62.07	96.99
10	33.61	33.61	42.22	46.8	55.56	86.82
11	39.70	39.7	49.87	55.28	65.63	102.5
12	24.96	32.66	41.03	45.48	54.00	84.37
13	2.821	21.55	27.07	30.01	35.63	55.67
14	2.818	19.11	24.01	26.62	31.60	49.38
15	2.843	21.73	27.30	30.26	35.92	56.13
16	2.948	22.64	28.44	31.53	37.43	58.48
17	2.918	21.18	26.61	29.49	35.01	54.71
18 (full)	2.910	21.14	26.56	29.45	34.96	54.62
PID	80.00	80.00	100.5	111.4	132.3	206.7
$\mathcal{H}_{\infty SISO}$	21.45	21.45	26.95	29.87	35.46	55.41

compared to the simulations. The second was to record the *average task execution time* (TET)—the time it takes the hardware to perform calculations from one time-step to the next. This can be considered a measurement of the computational complexity of the controller, and is a lower limit on the step-size. Any lower than this and the hardware will not be able to meet its deadline and stop its execution.

The experiments were performed in the setup shown in Fig. 1. The closed loop frequency response and step-response of the original controller K compared to the reduced controllers K_{10} and K_8 is given in Fig. 8. The average TET for the various controllers and solver types are given in Table 4. The system was run with step-size $h = 40 \mu\text{s}$, and only the modes that are stable at this step-size were tested. That is, the modes in Table 3 where $h_{max} \geq 40 \mu\text{s}$.

7. DISCUSSION

7.1 Model Reduction and Computational Complexity

From the model reduction it is seen that the original 18th-order controller can be reduced to a 10th-order model with no noticeable difference in the experimental step-response or closed-loop frequency response as seen in Fig. 8. Additionally, it was shown to maintain robust stability, thus it is a very viable controller choice. In terms of the impact on computational complexity, there is a 25.5% reduction – from 20.11 to 14.99 μs – if the erk8 solver is used for both controllers.

From Table 3 we can see that the 10th-order controller can run using the erk3 solver at a step-size of $h = 40 \mu\text{s}$, while the full 18th-order \mathcal{H}_{∞} MIMO controller needs erk8 for stability at this step-size. By choosing erk3 for the 10th-order controller we can see from Table 4 that this reduces the execution time to 10.71 μs , or a 46.7% reduction from the original controller.

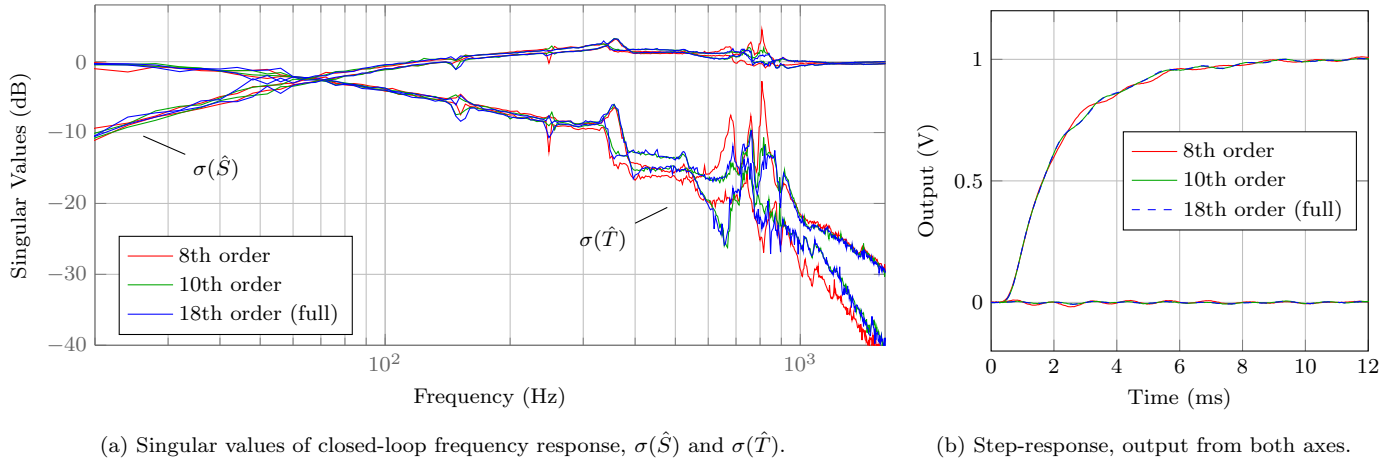


Fig. 8. Experimental frequency response and step response comparison for selected reduced order controllers.

Table 4. Average task execution time (TET) with different controller model order and solver types which gives an indication on the computational complexity. Step-size $h = 40 \mu\text{s}$. Dash (-) unstable, not tested.

Order	Average TET [μs]				
	erk1	erk2	erk3	erk5	erk8
≤ 7	-	-	-	-	-
8	-	10.25	10.43	11.10	13.64
9	-	-	10.55	11.43	14.26
10	-	-	10.71	11.64	14.99
11	-	-	10.89	11.91	15.79
12	-	-	11.07	12.36	16.79
13	-	-	-	-	17.68
14	-	-	-	-	18.82
15	-	-	-	-	19.61
16	-	-	-	-	20.91
17	-	-	-	-	22.61
18	-	-	-	-	20.11
PID	-	9.95	9.98	10.13	11.12
$\mathcal{H}_{\infty SISO}$	-	-	-	-	14.58

It is also interesting to note that the execution time does not strictly decrease with increased controller order, e.g. the 17th to 18th-order controller. By inspecting the state-space model of each of these controllers, we notice that the 18th-order controller has a lot more zero-valued elements. We speculate that the compiler simplifies the arithmetic on these elements.

7.2 Eigenvalues and Stability

As we have seen, the eigenvalues of the controller are one of the decisive factors for stability of an applied ERK method. Hence, it is important to consider how controller reduction changes the eigenvalues, especially for a fast and stiff system such as our lateral positioning platform of an AFM. The eigenvalues of our controller tended to become smaller in size with reduced orders, but this need not be the case. One should be careful when performing model reduction and always verify that the eigenvalues are within the stable region of the solver considered.

We have also seen how increased solver order increases the stability region, but at the same time it increases

the execution time. This will ultimately be a trade-off between moving the lower limit (due to computation time) and the upper limit (for stability) of the step-size, as illustrated in Fig. 9. Halving the step-size usually doubles the computational complexity (per unit of time), while increasing the solver order is harder to predict, but will generally depend on the controller order.

Note that we have not considered the accuracy of the solver methods. This is because we have assumed that the system is stiff, and stiff systems are characterized by becoming unstable before accuracy issues arise.

7.3 Robustness

The \mathcal{H}_{∞} norm of the sensitivity function S is a good measurement of robustness. It can be seen in Fig. 8 that the 8th order controller has worse characteristics in this regard, while the 10th order controller is almost identical to the original 18th order controller. This was as expected from the analysis during the controller design process. The sensitivity function is also the closed-loop response from disturbances at the output to the measured output. We can see that the system is extra sensitive to such disturbances in the 200-400 Hz range, which corresponds to the two smaller unmodeled resonant peaks along the x - and y -axis as can be seen in Fig. 2.

We have not treated discrete-time controllers in this paper. Such controllers can be obtained either through discrete-time controller design or continuous-to-discrete-time conversion methods. The comparison of such controllers to the results presented here is a topic for further studies.

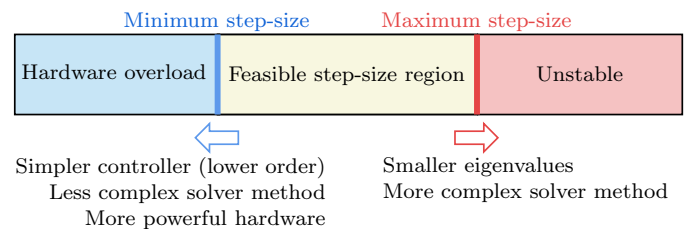


Fig. 9. Illustration of the trade-off between various factors for a real-time controller implementation.

8. CONCLUSION

In this paper we study some practical issues for a controller running in real-time. Since the capability of hardware is limited in terms of computational performance, a complex controller can become difficult to implement with a step-size small enough for stability. We have shown how to determine the maximum step-size a controller requires for numerical stability. Additionally, we discuss the effect of model reduction on stability, performance, and computational complexity.

In order to discuss these topics, a robustly stable \mathcal{H}_∞ controller was designed for a nanopositioning device. We showed that the numerical stability of an explicit Runge-Kutta method is determined by the eigenvalues of the controller. Model reduction was performed on the controller and the reduced controllers were compared in terms of performance and stability both in simulations and experiments which showed that the 18th-order controller could be reduced to a 10th-order model without any significant reduction in performance or stability. After the reduction process, the largest eigenvalues were reduced in size. So not only does the controller become computationally less complex, but the reduction process also allowed for larger step-sizes or alternatively simpler solver methods. Thus, both the lower and upper limit for implementability illustrated in Fig. 9 could be moved by controller reduction.

To summarize our points, we suggest the following implementation procedure in order to make a good solver choice and find a feasible step-size:

- (1) Design a controller and perform model reduction.
- (2) Find the maximum step-size providing stability for one or more chosen ERK methods such that (10) is satisfied for all eigenvalues of the controller.
- (3) An initial solver choice can be taken as the one which provides the best maximum step-size to computational complexity ratio. A rough estimate of the computational complexity can be found by simulations.
- (4) Run the controller at slightly below the maximum step-size, and reduce the step-size until the hardware is unable to perform the required calculations in time.
- (5) If no feasible step-size was found, one can reduce additional states or try another ERK method.

If this procedure was unsuccessful, one could try to design a controller with simpler structure or consider upgrading the hardware for more computational power.

REFERENCES

- Anderson, B.D.O. (1993). Controller design: moving from theory to practice. *IEEE Control Systems*, 13(4), 16–25.
- Anderson, B.D.O. and Liu, Y. (1989). Controller reduction: concepts and approaches. *IEEE Transactions on Automatic Control*, 34(8), 802–812.
- Aphale, S.S., Bhikkaji, B., and Moheimani, S.O.R. (2008). Minimizing scanning errors in piezoelectric stack-actuated nanopositioning platforms. *Nanotechnology, IEEE Transactions on*, 7(1), 79–90.
- Ascher, U.M. and Petzold, L.R. (1998). *Computer methods for ordinary differential equations and differential-algebraic equations*. Society for Industrial and Applied Mathematics, Philadelphia.
- Croft, D., Shed, G., and Devasia, S. (2001). Creep, Hysteresis, and Vibration Compensation for Piezoactuators: Atomic Force Microscopy Application. *Journal of Dynamic Systems, Measurement, and Control*, 123(1), 35–43.
- Dong, J., Salapaka, S.M., and Ferreira, P.M. (2007). Robust MIMO control of a parallel kinematics nano-positioner for high resolution high bandwidth tracking and repetitive tasks. *Decision and Control, 2007. 46th IEEE Conference on*, 4495–4500.
- Dormand, J.R. and Prince, P.J. (1980). A family of embedded Runge-Kutta formulae. *Journal of Computational and Applied Mathematics*, 6(1), 19–26.
- Egeland, O. and Gravdahl, J.T. (2002). *Modeling and Simulation for Automatic Control*. Marine Cybernetics, Trondheim, Norway.
- Eielsen, A.A., Vagia, M., Gravdahl, J.T., and Pettersen, K.Y. (2013). Damping and Tracking Control Schemes for Nanopositioning. *IEEE/ASME Transactions on Mechatronics*, 1–13.
- Eielsen, A.A., Gravdahl, J.T., and Pettersen, K.Y. (2012). Adaptive feed-forward hysteresis compensation for piezoelectric actuators. *The Review of scientific instruments*, 83(8), 085001.
- Fleming, A.J. (2010). Nanopositioning system with force feedback for high-performance tracking and vibration control. *Mechatronics, IEEE/ASME Transactions on*, 15(3), 433–447.
- Fleming, A.J., Aphale, S.S., and Moheimani, S.O.R. (2010). A new method for robust damping and tracking control of scanning probe microscope positioning stages. *Nanotechnology, IEEE Transactions on*, 9(4), 438–448.
- Hairer, E. and Wanner, G. (1996). *Solving Ordinary Differential Equations II*. Springer Berlin Heidelberg.
- Kaizuka, H. and Siu, B. (1988). A Simple Way to Reduce Hysteresis and Creep When Using Piezoelectric Actuators. *Japanese Journal of Applied Physics*, 27(Part 2, No. 5), L773–L776.
- Kuiper, S. and Schitter, G. (2012). Model-based feedback controller design for dual actuated atomic force microscopy. *Mechatronics*, 22(3), 327–337.
- Ladjal, H., Hanus, J.L., and Ferreira, A. (2009). H_∞ robustification control of existing piezoelectric-stack actuated nanomanipulators. *2009 IEEE International Conference on Robotics and Automation*, 3353–3358.
- Lee, C. and Salapaka, S.M. (2009). Fast Robust Nanopositioning: A Linear-Matrix-Inequalities-Based Optimal Control Approach. *Mechatronics, IEEE/ASME Transactions on*, 14(4), 414–422.
- Lyons, R.G. (2010). *Understanding Digital Signal Processing*. Prentice Hall, Upper Saddle River, NJ, 3rd edition.
- Obinata, G. and Anderson, B.D.O. (2001). *Model reduction for control system design*. Springer-Verlag New York, Inc.
- Prince, P.J. and Dormand, J.R. (1981). High order embedded Runge-Kutta formulae. *Journal of Computational and Applied Mathematics*, 7(1), 67–75.
- Ragazzon, M.R.P. (2013). *Nanopositioning in Atomic Force Microscopes: Robust Control Design, Order Reduction and Numerical Implementability*. Master's thesis, Norwegian University of Science and Technology.
- Salapaka, S. and Sebastian, A. (2003). Control of the nanopositioning devices. *Decision and Control, 2003. Proceedings. 42nd IEEE Conference on*, 3(December), 3644–3649.
- Salapaka, S., Sebastian, A., Cleveland, J.P., and Salapaka, M.V. (2002). High bandwidth nano-positioner: A robust control approach. *Review of Scientific Instruments*, 73(9), 3232.
- Schitter, G., Menold, P., Knapp, H.F., Allgöwer, F., and Stemmer, A. (2001). High performance feedback for fast scanning atomic force microscopes. *Review of Scientific Instruments*, 72(8), 3320.
- Schitter, G. and Stemmer, A. (2004). Identification and Open-Loop Tracking Control of a Piezoelectric Tube Scanner for High-Speed Scanning-Probe Microscopy. *IEEE Transactions on Control Systems Technology*, 12(3), 449–454.
- Sebastian, A. and Salapaka, S.M. (2005). Design methodologies for robust nano-positioning. *IEEE Transactions on Control Systems Technology*, 13(6), 868–876.
- Skogestad, S. and Postlethwaite, I. (2007). *Multivariable feedback control: analysis and design*. Wiley-Interscience, 2nd edition.
- Yong, Y.K., Liu, K., and Moheimani, S.O.R. (2010). Reducing cross-coupling in a compliant XY nanopositioner for fast and accurate raster scanning. *Control Systems Technology, IEEE Transactions on*, 18(5), 1172–1179.